Tristability of cavity magnon polaritons

M. X. Bi,[1] X. H. Yan,[2,*] Y. Zhang,[1,†] and Y. Xiao[1,‡]

[1]*College of Science, Nanjing University of Aeronautics and Astronautics, Nanjing 210016, China*

[2]*School of Material Science and Engineering, Jiangsu University, Zhenjiang, 212013, China*

(Received 26 September 2020; revised 24 February 2021; accepted 25 February 2021; published 8 March 2021)

We carry out a theoretical study of the nonlinear behavior of cavity magnon polaritons (CMPs) under strong microwave driving, with two kinds of nonlinearity being involved: either (i) the photon Kerr effect (PKE) and the magnon saturation effect (MSE) or (ii) the magnon Kerr effect (MKE) and the MSE. The effects arising in these two cases are similar for the lower polariton mode of CMPs but opposite for the upper polariton mode. In case (i), the dominant nonlinearity for the upper polariton mode of CMPs changes from the MSE to the PKE as the driving intensity increases, which can lead to two hysteresis loops in opposite directions and hence to tristability. In case (ii), however, the upper polariton mode exhibits only the usual bistability rather than tristability since the MKE is dominated by the MSE. In particular, there is no bistable behavior in the upper polariton mode when the two nonlinearities balance each other. The results of this study provide a possible basis for the practical manipulation and control of information via the double nonlinearities in a cavity-magnon system.

DOI: 10.1103/PhysRevB.103.104411

I. INTRODUCTION

Nonlinear optics associated with a dependence on driving strength, as a significant characteristic of the interaction between light and matter, has been extensively studied using various platforms in recent decades [1–19]. In one well-known example, a Kerr medium embedded in a device such as a cavity or other optical system is used to provoke optical nonlinearity [20–32]. Under high levels of excitation, the nonlinearity of the dynamics becomes so strong that the behavior of the system is greatly modified in ways that can be beneficial, for example, for the development of switches and logic devices for quantum computing and information processing [33–37]. The majority of applications in this field focus on the infrared or visible spectrum, and the excitation of nonlinearity at microwave frequencies has rarely been studied owing to the weak nonlinear susceptibility of materials. However, advances in materials science and processing technology have led to the development of artificial Kerr media, such as carbon-loaded composite materials, in which it is possible to stimulate an appreciable microwave photon Kerr effect (PKE) [38–42], which extends nonlinear optics from the visible and infrared regions down to microwave frequencies.

Lately, in the presence of magnetocrystalline anisotropy, the magnon Kerr effect (MKE) has been realized in an experimental configuration consisting of a small sphere of yttrium iron garnet (YIG) placed inside a microwave cavity [43–45]. This phenomenon has been explained theoretically [46–48] in terms of the cavity magnon polariton (CMP), which represents a new kind of hybridized quasiparticle [49–68] produced by the strong coupling between the microwave photons and the ferromagnetic insulator YIG with its high spin density and extremely low magnetic damping rate. In CMP, optical nonlinearity is induced by magnetic nonlinearity via photon-magnon interaction. Besides the MKE, another magnon nonlinear effect, i.e., the magnon saturation effect (MSE), was recently proposed [69]. In the MSE, the large-angle precession of magnetization at high excitation leads to a nonlinear attraction between two polariton modes and finally results in the saturation of magnons.

Based on these recent developments, in this paper, we theoretically predict nonlinear behavior of the cavity-magnon system, involving hybridization of two types of nonlinearities: either (i) the PKE and MSE or (ii) MKE and MSE. Our results indicate that the upper polariton mode of CMP can display tristability in case (i) but only the usual bistability in case (ii) since MSE dominates over MKE. These findings provide a means to manipulate the behavior of CMPs using the double nonlinearities.

The remainder of the paper is organized as follows. In Sec. II, we construct the model and present a comprehensive derivation of the intracavity field amplitude for cases (i) and (ii) based on the Heisenberg-Langevin equations in the steady state. In Sec. III, we discuss the numerical results based on the formulas derived in Sec. II. Our conclusions are presented in Sec. IV.

II. MODEL AND THEORY

A. Case (i): PKE and MSE

The model under consideration is a microwave cavity containing a small ferromagnetic insulator (FMI) sphere with $N \sim 10^{16}$ spins and two isotropic artificial Kerr-type media with the same size and high damage threshold, as sketched in

*xhyan@nuaa.edu.cn
†yingzhang@nuaa.edu.cn
‡fryxiao@nuaa.edu.cn

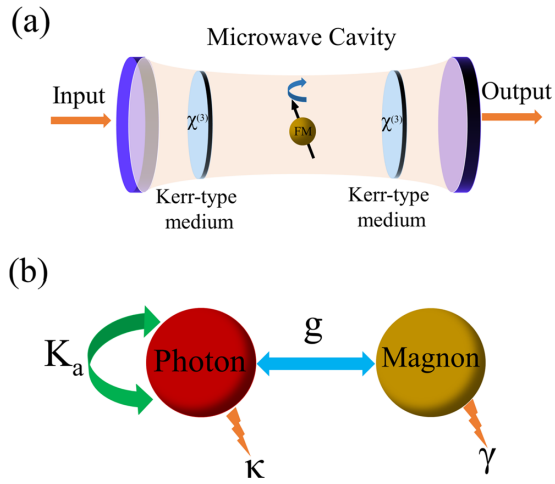

FIG. 1. (a) Schematic layout of the cavity-magnon system under study. The FMI sphere is positioned at the center of the microwave cavity, and two isotropic artificial Kerr-type media are placed symmetrically, one on each side of the sphere. "Input" and "Output" represent the incident and transmitted microwave driving fields, respectively. (b) Schematic representation of the interaction between the subsystems. The green arrow represents the PKE induced by the Kerr-type medium with photon Kerr coefficient K_a, while the blue arrow represents the coupling between the cavity photon with dissipation rate κ and the magnon with dissipation rate γ. g is the single-spin coupling strength.

Fig. 1. The FMI sphere is positioned at the center of the cavity to provide strong coupling at the maximum of the microwave magnetic field. The two isotropic artificial Kerr-type media, with intrinsic third-order nonlinear susceptibilities $\chi^{(3)}$, are used to induce the PKE in the microwave cavity and are placed symmetrically, one on each side of the FMI sphere, to ensure that the maximum of the magnetic field remains at the center. A microwave pump field is injected into the cavity from the left and comes out from the right.

The effective Hamiltonian of the system comprises four parts:

$$H_{K_AS} = H_c + H_{K_A} + H_m + H_I + H_d, \tag{1}$$

where $H_c = \omega_c a^\dagger a$ (in units of $\hbar = 1$) is the bare Hamiltonian for the single-cavity mode with creation (annihilation) operator $a^\dagger$ (a) at frequency ω_c. The Hamiltonian of the photon Kerr nonlinearity is [20]

$$H_{K_A} = \frac{1}{2}\int \varepsilon_{K_a}(\mathbf{r},t)E^2(\mathbf{r},t)\,d\mathbf{r}, \tag{2}$$

where $E(\mathbf{r},t) = E_0(\mathbf{r})[a(t) + a^\dagger(t)]$ is the electrical component of the microwave field with amplitude $E_0(\mathbf{r})$ at $\mathbf{r}$ and $\varepsilon_{K_a}(\mathbf{r},t) = \varepsilon_0\chi^{(3)}E^2(\mathbf{r},t)$ is the nonlinear part of the permittivity induced by the isotropic artificial Kerr-type medium, with ε_0 and $\chi^{(3)}$ being the vacuum permittivity and third-order nonlinear susceptibility, respectively. Neglecting the rapidly oscillating and perturbation terms, we can express the second-quantized form of Eq. (2) as

$$H_{K_A} = K_a a^\dagger a a^\dagger a, \tag{3}$$

where $K_a = \int \varepsilon_0\chi^{(3)}E_0^4(\mathbf{r})\,d\mathbf{r}$ is the photon Kerr coefficient related to the third-order nonlinear susceptibility, the amplitude of the electric field, and the volume of the Kerr-type medium.

A uniform static magnetic field $\mathbf{H} = H\mathbf{e}_z$ along the z direction is applied to the FMI sphere of volume V_m to align the magnetization and tune the uniform precession mode (i.e., Kittel mode) frequency, resulting in a Zeeman energy

$$H_m = -\mu_0\int_{V_m}\mathbf{M}\cdot\mathbf{H}\,d\rho = -B_0M^zV_m, \tag{4}$$

where $\mathbf{M} = (M^x, M^y, M^z)$ is the macrospin magnetization of the FMI sphere. The macrospin magnetization $\mathbf{M}$ and macrospin operator $\mathbf{S}$ are related by [49]

$$\mathbf{M} = -\frac{\gamma_s\mathbf{S}}{V_m} = -\frac{\gamma_s\sum_j\mathbf{s}_j}{V_m} = -\frac{\gamma_s}{V_m}(S^x, S^y, S^z), \tag{5}$$

where $\mathbf{s}_j$ is the jth spin in the FMI sphere and γ_s is the gyromagnetic ratio, and on inserting this relation into Eq. (4), we obtain

$$H_m = \omega_m S^z, \tag{6}$$

with $\omega_m = \gamma_s\mu_0H = \gamma_{gr}H$.

Using the rotating-wave approximation (RWA) [70], the Hamiltonian for the coupling between a microwave photon and the FMI sphere via the magnetic-dipole interaction can be written as [69]

$$H_I = ig(a^\dagger S^- - S^+a), \tag{7}$$

where g is the single-spin coupling strength and $S^\pm = S^x \pm iS^y$ are the spin raising and lowing operators. Moreover, a microwave driving field is applied to the cavity, leading to

$$H_d = \Omega(a^\dagger e^{-i\omega t} + ae^{i\omega t}), \tag{8}$$

with Ω and ω being the driving field amplitude and the driving frequency, respectively. Therefore, the full effective Hamiltonian for Eq. (1) can be expressed as

$$\begin{aligned}H_{K_AS} =& \omega_m S^z + \omega_c a^\dagger a + K_a a^\dagger a a^\dagger a + ig(a^\dagger S^- - S^+a)\\ &+ \Omega(a^\dagger e^{-i\omega t} + ae^{i\omega t}).\end{aligned} \tag{9}$$

In the rotating frame of the driving frequency ω, the Hamiltonian (9) is transformed to

$$\begin{aligned}H'_{K_AS} =& -\Delta_m S^z - \Delta_c a^\dagger a + K_a a^\dagger a a^\dagger a + ig(a^\dagger S^- - S^+a)\\ &+ \Omega(a^\dagger + a),\end{aligned} \tag{10}$$

where $\Delta_{m(c)} = \omega - \omega_{m(c)}$ is the magnon (photon) frequency detuning relative to the driving frequency.

From Eq. (10), by inserting the dissipation terms κ and γ for the photon and magnon, respectively, the Heisenberg-Langevin equations can be obtained for the steady state as follows:

$$\frac{d\langle a\rangle}{dt} = [i(\Delta_c - 2K_a\langle a^\dagger\rangle\langle a\rangle) - \kappa]\langle a\rangle + g\langle S^-\rangle - i\Omega, \tag{11a}$$

$$\frac{d\langle S^-\rangle}{dt} = (i\Delta_m - \gamma)\langle S^-\rangle + 2g\langle S^z\rangle\langle a\rangle, \tag{11b}$$

$$\frac{d\langle S^z\rangle}{dt} = -\gamma\left(\langle S^z\rangle + \tfrac{1}{2}N\right) - g(\langle a^\dagger\rangle\langle S^-\rangle + \langle S^+\rangle\langle a\rangle), \tag{11c}$$

where $\langle\cdots\rangle$ represents the expectation value of an operator. To simplify numerical calculations, the following transformations of variables are made: $\langle a\rangle = \sqrt{N}\alpha$, $\langle S^-\rangle = NS$, and $\langle S^z\rangle = NS^z$. Here, the mean-field treatment neglects the quantum fluctuation, indicating that our theory is a semiclassical one. Equations (11a)–(11c) then take the simplified form

$$\frac{d\alpha}{dt} = [i(\Delta_c - 2K_A|\alpha|^2) - \kappa]\alpha + GS - i\eta, \tag{12a}$$

$$\frac{dS}{dt} = (i\Delta_m - \gamma)S + 2GS^z\alpha, \tag{12b}$$

$$\frac{dS^z}{dt} = -\gamma\left(S^z + \tfrac{1}{2}\right) - G(\alpha^* S + S^*\alpha), \tag{12c}$$

with $G = g\sqrt{N}$, $K_A = K_a N$, and $\eta = \Omega/\sqrt{N}$. In the steady state for Eqs. (12a)–(12c), i.e., $d\alpha/dt = 0$, $dS/dt = 0$ and $dS^z/dt = 0$, we have

$$\frac{|\eta|^2}{|\alpha|^2} = \left[(\Delta_c - 2K_A|\alpha|^2) - \Delta_m \frac{G^2}{\Delta_m^2 + \gamma^2(1 + 4G^2|\alpha|^2/\gamma^2)}\right]^2 + \left[\kappa + \gamma \frac{G^2}{\Delta_m^2 + \gamma^2(1 + 4G^2|\alpha|^2/\gamma^2)}\right]^2, \tag{13}$$

which combines the driving field amplitude η and the intracavity field amplitude $|\alpha|^2$. As $K_A = 0$, Eq. (13) describes the case with only MSE that was studied in our previous work [69].

B. Case (ii): MKE and MSE

The second case is a single FMI placed in the microwave cavity so that no PKE is present. Meanwhile, the MKE due to strong magnetocrystalline anisotropy of FMI is involved. Therefore, the total Hamiltonian containing MKE and MSE can be expressed as

$$H_{K_M S} = H_c + H_m + H_{K_M} + H_I + H_d, \tag{14}$$

where H_c, H_m, H_I, and H_d are the same as in Sec. II A. The Hamiltonian

$$H_{K_M} = -\frac{\mu_0}{2}\int_{V_m} \mathbf{M}\cdot\mathbf{H}_{\rm an}\, d\rho \tag{15}$$

represents the magnetocrystalline anisotropy energy, with μ_0 and $\mathbf{H}_{\rm an}$ respectively denoting the vacuum permeability and the anisotropic field resulting from the magnetocrystalline anisotropy in the FMI sphere. The anisotropic field is given by [43,44,46,71,72]

$$\mathbf{H}_{\rm an} = -\frac{\tau^x K_{\rm an} M^x}{M^2}\mathbf{e}_x - \frac{\tau^y K_{\rm an} M^y}{M^2}\mathbf{e}_y - \frac{\tau^z K_{\rm an} M^z}{M^2}\mathbf{e}_z, \tag{16}$$

where $K_{\rm an}$ is the dominant first-order anisotropy constant, M is the saturation magnetization, and $\tau^{x(y,z)}$ is a dimensionless parameter that depends on the angle between the crystallographic axis and the uniform external static magnetic field. Inserting Eqs. (5) and (16) into Eq. (15), we have

$$H_{K_M} = K_x(S^x)^2 + K_y(S^y)^2 + K_z(S^z)^2, \tag{17}$$

where $K_{(x,y,z)} = \tau^{(x,y,z)}\mu_0 K_{\rm an}\gamma_s^2/2M^2V_m$ are the magnon Kerr coefficients in the (x, y, z) directions. Using the RWA [70], the total effective Hamiltonian for Eq. (14) can then be obtained as

$$H_{K_M S} = \omega_m S^z + \omega_c a^\dagger a + \frac{K_x + K_y}{4}(S^+S^- + S^-S^+) + K_z(S^z)^2 + ig(a^\dagger S^- - S^+ a) + \Omega(a^\dagger e^{-i\omega t} + a e^{i\omega t}). \tag{18}$$

After transformation to the rotating frame with respect to the driving frequency ω, the Hamiltonian (18) can be rewritten as

$$H'_{K_M S} = -\Delta_m S^z - \Delta_c a^\dagger a + \frac{K_x + K_y}{4} \times (S^+S^- + S^-S^+) + K_z(S^z)^2 + ig(a^\dagger S^- - S^+ a) + \Omega(a^\dagger + a). \tag{19}$$

Solving the equations of motion for Eq. (19) in the steady state, we obtain

$$S^z = -\frac{1}{2\left[1 + \dfrac{4G^2|\alpha|^2}{\gamma^2 + (\Delta_m - 2K_M S^z)^2}\right]} \tag{20}$$

and

$$\frac{|\eta|^2}{|\alpha|^2} = \left[\Delta_c + \frac{2G^2 S^z(\Delta_m - 2K_M S^z)}{\gamma^2 + (\Delta_m - 2K_M S^z)^2}\right]^2 + \left[\kappa - \frac{2G^2\gamma S^z}{\gamma^2 + (\Delta_m - 2K_M S^z)^2}\right]^2, \tag{21}$$

with $G = \sqrt{N}g$, $K_M = (2K_z - K_x - K_y)N/2$, and $\eta = \Omega/\sqrt{N}$. By combining Eqs. (20) and (21), we can obtain the relationship between η and $|\alpha|^2$.

We have now derived the essential formulas for both cases, which paves the way for later analysis and discussion. In this paper, we focus on the positive PKE and MKE, i.e., $K_A > 0$ and $K_M > 0$.

III. RESULTS AND DISCUSSION

A. Only PKE

In the limit of extremely low excitation, the contributions of the nonlinearities to the system are negligible, and thus, the behavior of the system is determined by the harmonic oscillators. The frequency spectrum of the CMPs in this limit is shown in Fig. 2(a), where a typical level repulsion with a gap of $2G/2\pi$ between the lower and upper polariton modes can be clearly seen when the magnon mode is tuned to cross the cavity mode. The parameters in our calculation are $G/2\pi = 8$ MHz, $\kappa/2\pi = \gamma/2\pi = 0.7$ MHz, $\kappa_a/2\pi = 0.6$ MHz, $\omega_c/2\pi = 10$ GHz, and $\omega_m = \gamma_{\rm gr}H$, where $\gamma_{\rm gr}/2\pi = 28\mu_0$ GHz/T is the gyromagnetic ratio. Figure 2(b) shows the intracavity field amplitude $|\alpha|^2$ versus the detuning $\Delta_c/2\pi$ under weak driving power, namely, $P_d = 1.4$ mW, when the magnetic field is fixed at $\mu_0 H = 357.1$ mT (i.e., $\omega_m = \omega_c$), as shown by the vertical dashed red line in Fig. 2(a). A clear Rabi splitting appears, in which the left and right peaks correspond to the lower and upper polariton modes of the CMPs, respectively, and are separated by $2G/2\pi$.

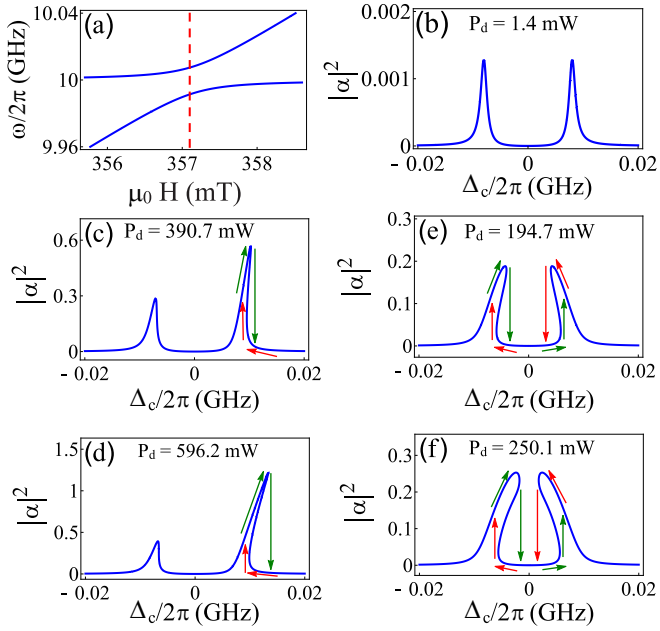

FIG. 2. (a) Frequency spectra of CMPs versus magnetic field. The vertical dashed red line indicates the resonance between the photon and magnon. (b) Intracavity amplitude $|\alpha|^2$ versus detuning $\Delta_c/2\pi$ at $P_d = 1.4$ mW (without any nonlinearity). (c) and (d) $|\alpha|^2$ in the presence of only PKE (without MSE) at 390.7 and 596.2 mW, respectively. (e) and (f) $|\alpha|^2$ in the presence of only MSE (without PKE) at 194.7 and 250.1 mW, respectively. The green and red arrows indicate forward and backward sweeps, respectively.

To better understand the behavior of the system subject to these two nonlinear effects, i.e., PKE and MSE, we first separate them from each other and then analyze the influence of each nonlinearity on the system. Figures 2(c) and 2(d) show the responses of the intracavity field amplitude $|\alpha|^2$ to only the PKE, respectively, at high excitation. In Fig. 2(c), where $K_A/2\pi = 3.5$ MHz, the two Rabi peaks bend to the right and become unequal in height when $P_d = 390.7$ mW. It can be seen that bistability occurs mainly in the right peak with a clockwise hysteresis loop (indicated by the green and red arrows) owing to the predominance of the anharmonic oscillators resulting from the PKE under strong driving power. The left peak does not exhibit bistability, as can be seen from the remarkably small tilt compared with the right peak. When the driving power reaches 596.2 mW, the right peak bends to the right more obviously with a larger hysteresis loop emerging, as shown in Fig. 2(d). This is due to the larger PKE being excited by the strong driving field. However, the left peak still presents a weak response to the strong driving. Using the mean-field approximation, the photon Kerr term in Eq. (10) can be expressed as $\Delta_{K_A} a^\dagger a$, where $\Delta_{K_A} = 2K_A|\alpha|^2$ is the photon frequency shift. This gives rise to a blueshift of the effective photon frequency $\omega_{c,\mathrm{eff}} = \omega_c + \Delta_{K_A}$. This frequency shift increases the weight of the photon component in the right peak and thereby promotes the occurrence of bistability in the right peak. In contrast, this frequency shift decreases the weight of the photon component in the left peak, thereby weakening the photon Kerr effect.

From the normal-mode perspective, Eq. (13) can be simplified to

$$\left|\frac{\alpha}{\eta}\right|^2 = \left|\frac{\lambda_+}{\Omega_+^{K_A} - i\Delta_c} + \frac{\lambda_-}{\Omega_-^{K_A} - i\Delta_c}\right|^2, \tag{22}$$

where

$$\lambda_+ = \frac{\Omega_+^{K_A} - \gamma}{\Omega_+^{K_A} - \Omega_-^{K_A}}, \quad \lambda_- = \frac{\Omega_-^{K_A} - \gamma}{\Omega_-^{K_A} - \Omega_+^{K_A}}, \quad \Omega_\pm^{K_A} = \frac{\kappa + \gamma}{2} + i[K_A|\alpha|^2 \pm \sqrt{G^2 + (K_A|\alpha|^2)^2}]. \tag{23}$$

The system under extremely low microwave driving (i.e., when $|\alpha|^2$ is very small) resembles two coupled harmonic oscillators. The normal modes $\Omega_\pm^{K_A}$ corresponding to the right and left peaks in Fig. 2(b) are located at $\Delta_c/2\pi = \pm G/2\pi$. However, these two normal modes gradually tilt to the right as the driving intensity increases. At sufficiently high excitation (i.e., when $|\alpha|^2$ is very large), the left peak gets close to $\Delta_c/2\pi = 0$, which is the limit that it can reach. However, there is no limit to the tilt of the right peak because of the photonlike upper polariton mode resulting from the blueshift of the effective photon frequency.

B. Only MSE

When we consider only the MSE by setting $K_A/2\pi = 0$ GHz in Figs. 2(e) and 2(f), the nonlinear behavior is quite different from that in Figs. 2(c) and 2(d). When the driving intensity becomes strong, e.g., $P_d = 194.7$ mW, the two Rabi peaks attract each other and simultaneously exhibit bistability, as shown in Fig. 2(e), which is a signature of MSE [69]. It is not difficult to find that the bistability displays a clockwise hysteresis loop for the left peak but a counterclockwise hysteresis loop for the right peak. As the driving power increases further to 250.1 mW, the bistability of the two peaks becomes more obvious, as shown in Fig. 2(f). At a very high level of driving power, two tilted peaks will merge with each other and become a single peak at the cavity resonance frequency, i.e., $\Delta_c/2\pi = 0$ GHz. This limiting behavior at ultrahigh power indicates the magnon saturation effect which was studied in our recent work on cavity magnon polariton [69]. When the power is high enough, i.e., the photon number is very large, the spins are all excited. Therefore, there are no available spins to couple with photons so that the spin system does not contribute to the spin-photon dynamics. This behavior is analogous to the interaction between many atoms and a cavity at high power [9]. It is possibly difficult to observe the limiting case with a single peak in experiment. This is because many other nonlinear interactions may start to contribute when the magnon number is huge. In this work, we do not study this limiting case of MSE but consider the combined effect of MSE and PKE or MKE on magnon-photon dynamics at intermediate power.

We can understand the nonlinear behavior of MSE by solving for the normal modes from Eq. (13):

$$\Omega_\pm^S = \frac{\kappa + \gamma}{2} \pm i\sqrt{\frac{G^2}{1 + 4G^2|\alpha|^2/(\Delta_c^2 + \gamma^2)}}, \tag{24}$$

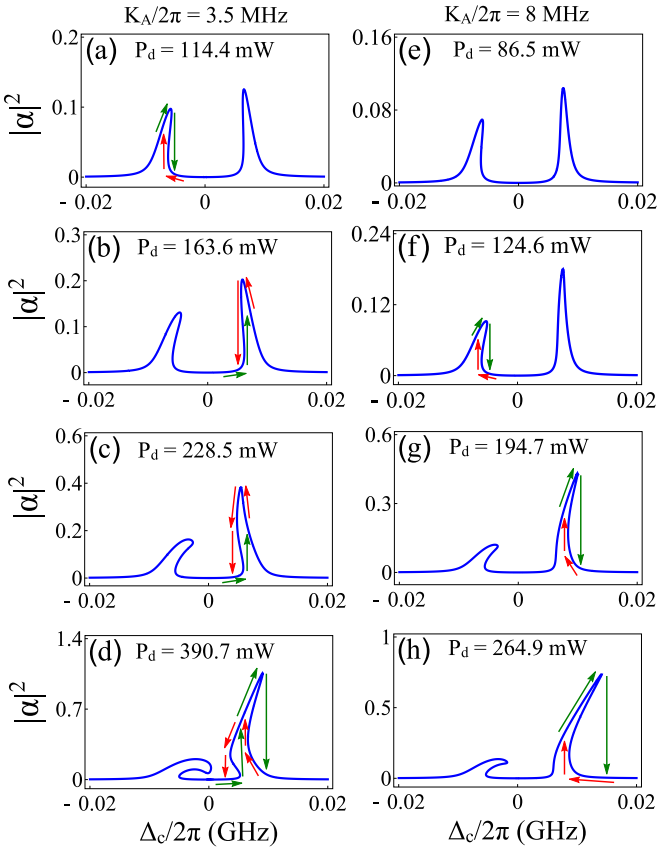

FIG. 3. (a)–(h) $|\alpha|^2$ versus $\Delta_c/2\pi$ for various P_d. The left and right panels are for $K_A = 3.5$ and 8 MHz, respectively. The green and red arrows indicate forward and backward sweeps, respectively.

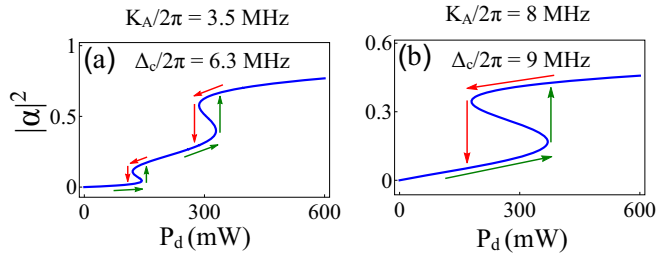

FIG. 4. (a) and (b) $|\alpha|^2$ versus P_d for $\Delta_c/2\pi = 6.3$ and 9 MHz, respectively. The left and right panels are for $K_A = 3.5$ and 8 MHz, respectively. The green and red arrows indicate forward and backward sweeps, respectively.

which corresponds to the Rabi peaks in Fig. 2(b) at ultralow excitation. When the driving intensity increases (i.e., $|\alpha|^2$ becomes larger), the behavior of the system is governed by the anharmonic oscillators, and consequently, $\Omega_{\pm}^{S}$ moves to the cavity resonance frequency, i.e., $\Delta_c/2\pi = 0$.

Up to this point, we have discussed the effect of each nonlinear effect on the system under strong microwave driving. In brief, the behavior induced by the PKE exhibits a tendency to bend to the right for both Rabi peaks. However, the MSE results in the attraction of the two peaks. Consequently, the two nonlinearities have similar influences on the left peak but opposite influences on the right peak. Therefore, as both nonlinear effects are involved inside a system, some novel physical phenomena may appear, which will be explored later.

C. PKE and MSE

We first discuss the behavior in the presence of both the PKE and the MSE under strong driving field. Figure 3 shows the intracavity field amplitude $|\alpha|^2$ versus the detuning $\Delta_c/2\pi$ for various driving powers P_d. The left panels in Fig. 3 are for a small photon Kerr coefficient, namely, $K_A/2\pi = 3.5$ MHz. When $P_d = 114.4$ mW, as shown in Fig. 3(a), the two Rabi peaks are attracted to each other in response to the nonlinearity. The left peak exhibits bistability with clockwise hysteresis loops, but the bistability in the right peak is not obvious. In addition, two intriguing phenomena occur. First, the two peaks become asymmetric, with the right peak being higher than the left peak. Here, the PKE induces a blueshift of the effective photon frequency and thus results in a larger photon component in the right peak than in the left peak. Second, the tilt of the left peak is larger than that of the right peak. The reason for this is that the two nonlinearities have similar effects on the left peak but opposite effects on the right peak. As for a stronger driving field, e.g., $P_d = 163.6$ mW, the left peak becomes more tilted, and the right peak displays bistability with counterclockwise hysteresis loops as the MSE dominates in the right peak, as shown in Fig. 3(b). With a further increase in driving power, the competition between PKE and MSE becomes stronger and stronger, as shown in Fig. 3(c). When the driving power P_d is increased to 390.7 mW, as shown in Fig. 3(d), the tilt of the left peak becomes more pronounced than in Figs. 3(a)–3(c). The right peak is now changed to tilt to the right, which gives rise to two opposite hysteresis loops: a counterclockwise loop arising from the MSE and a clockwise loop arising from the PKE. The occurrence of these two hysteresis loops generates tristability in the right peak due to the competition between the two nonlinear effects.

The right panels in Fig. 3 are for a larger photon Kerr coefficient, namely, $K_A/2\pi = 8$ MHz. As the PKE becomes strong, it dominates over the MSE, and therefore, the nonlinear behavior is close to that of PKE, as shown in Figs. 3(e)–3(h). In this regime, the PKE dominates over the MSE. The normal modes can be written as

$$\Omega_{\pm}^{K_A S} = \frac{\kappa+\gamma}{2} + i\left[K_A|\alpha|^2 \pm \sqrt{(K_A|\alpha|^2)^2 + \frac{G^2}{1+4G^2|\alpha|^2/(\Delta_c^2+\gamma^2)}}\right], \quad (25)$$

where $K_A|\alpha|^2$ and $4G^2|\alpha|^2/(\Delta_c^2+\gamma^2)$ arise from the PKE and MSE, respectively. We find that the left normal mode always satisfies the relation $-G < \mathrm{Im}(\Omega_{-}^{K_A S}) < 0$. This indicates that both nonlinearities make the left peak tilt to the right. However, there exists a competition in the right normal mode $\Omega_{+}^{K_A S}$ between two nonlinear effects. With an increase in the driving power, the right peak begins to tilt, with the direction of tilt depending on the relative strengths of the nonlinear effects.

We next undertake a qualitative analysis of the behavior of the right peak ($\Delta_c = G$) shown in Fig. 3. First, we assume that the change due to nonlinearity is not so large that

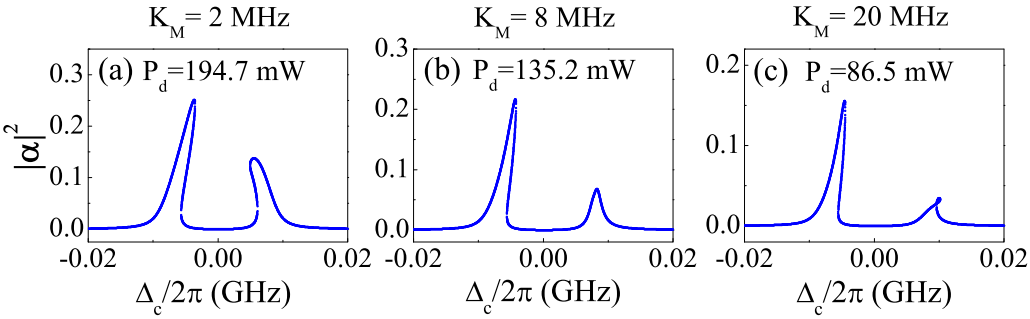

FIG. 5. (a)–(c) $|\alpha|^2$ versus $\Delta_c/2\pi$ for various values of K_M.

$G^2/(\Delta_c^2+\gamma^2)\approx 1$ still holds. Second, we Taylor expand Eq. (25) and obtain

$$\mathrm{Im}(\Omega_+^{K_AS}) = K_A|\alpha|^2 + \sqrt{(K_A|\alpha|^2)^2 + G^2(1-4|\alpha|^2)}. \quad (26)$$

In order to see the frequency shift around G, we solve the equation $\mathrm{Im}(\Omega_+^{K_AS}) = G$ and obtain $(K_A - 2G)|\alpha|^2 = 0$. One can clearly see that for $K_A < 2G$, the MSE is dominant and the right peak first tilts to the left, i.e., $\mathrm{Im}(\Omega_+^{K_AS}) < G$, leading to the bistability shown in Figs. 3(b) and 3(c). With a further increase in the driving power, $|\alpha|^2$ increases, and the PKE becomes dominant. Based on Eq. (26), the term $K_A|\alpha|^2$ increases and finally results in $\mathrm{Im}(\Omega_+^{K_AS}) > G$. That is to say, the right peak tilts to the right, and the tristability appears as seen in Fig. 3(d). For a larger K_A that still satisfies $K_A < 2G$, although the dominance of the MSE can still induce a tilt to the left at first, the larger PKE rapidly balances the MSE so that the right peak does not produce the tristability.

The behavior of tristability can be further appreciated when checking the intracavity field amplitude $|\alpha|^2$ versus the driving power P_d at fixed detuning. As P_d increases, the nonlinear behavior is initially determined by the MSE, which gives rise to the first hysteresis loop. With a further increase in P_d, the strength of the PKE exceeds that of the MSE, and hence, a second hysteresis loop appears. Consequently, tristability occurs, as can be seen in Fig. 4(a). However, for a larger K_A, as shown in Fig. 4(b), only one hysteresis loop arises due to stronger PKE than MSE.

D. MKE and MSE

Figure 5 shows the results in the presence of MKE and MSE for various magnon Kerr coefficients K_M. One can see that the left peak tilts to the right, which is similar to the results in case (i). But the difference is that the height of the left peak is higher than that of the right peak. This is because of the blueshift of the effective magnon frequency, resulting in a larger weight of photon components of the lower polariton mode. Like for Eq. (25), we can write

$$\Omega_\pm^{K_MS} = \frac{\kappa+\gamma}{2} + i\left\{\frac{K_M(1+2S^z)}{2} \pm \sqrt{-2G^2S^z + \frac{[K_M(1+2S^z)]^2}{4}}\right\}, \quad (27)$$

where $K_M(1+2S^z)$ and $-2G^2S^z$ correspond to the MKE and MSE, respectively. It is obvious that the relation $-G < \mathrm{Im}(\Omega_-^{K_MS}) < 0$ always holds for the left normal mode $\Omega_-^{K_MS}$, which suggests that the left peak always tilts to the right. However, the competition occurs for the right normal mode $\Omega_+^{K_MS}$. Assuming that $\mathrm{Im}(\Omega_+^{K_MS}) = G$, we have $(K_M - G)(1 + 2S^z) = 0$. For $K_M < G$ shown in Fig. 5(a), the right peak tilts to the left owing to the dominance of the MSE. As $K_M = G$ [Fig. 5(b)], there is no tilt for the right peak without any bistability due to the cancellation of two nonlinearities. When $K_M > G$, the MKE plays a crucial role, reproducing tilt to the right for the right peak shown in Fig. 5(c). Here, we should emphasize that the mechanisms leading to tristability in case (i) and bistability in case (ii) are different. As can be deduced from Eq. (20), S^z changes from $-\frac{1}{2}$ to 0 with increasing intracavity field amplitude $|\alpha|^2$, which means that the direction of the macroscopic spin rotates from vertical to in plane. In this process, the PKE used in case (i), i.e., $K_a|\alpha|^2$, is unrelated to S^z. However in case (ii), both MKE and MSE are determined by S^z, which greatly suppresses the occurrence of tristability.

IV. CONCLUSIONS

In conclusion, we have investigated the response of a cavity-magnon system to double nonlinear effects under strong microwave driving. In plots of field amplitude versus detuning, the left Rabi peak always tilts to the right as a result of the similar effects of the two nonlinearities. For the right Rabi peak, however, the two nonlinearities have opposite effects, and the competition between them induces a variety of nonlinear behaviors. In case (i), where the PKE and MSE are present, the right peak tilts to the left at first, owing to the dominance of the MSE, and then to the right as the PKE becomes dominant, resulting in tristability. In case (ii), where the MKE and MSE are present, the right peak tilts only to the left or only to the right, depending on the value of the magnon Kerr coefficient, which leads to the usual bistability instead of tristability. In some case, the MKE and MSE cancel each other, reproducing no tilt. Our research results have revealed a double nonlinear dynamics in the cavity-magnon system, which may have applications to information processing and to novel spintronics applications.

ACKNOWLEDGMENTS

This work is supported by the National Natural Science Foundation of China (Grants No. 61974067 and No. 11804158). We thank Prof. J. Q. You and Prof. C.-M. Hu for helpful suggestions and comments.

[1] D. A. Kleinman, Nonlinear Dielectric Polarization in Optical Media, Phys. Rev. **126**, 1977 (1962).

[2] J. A. Armstrong, N. Bloembergen, J. Ducuing, and P. S. Pershan, Interactions between Light Waves in a Nonlinear Dielectric, Phys. Rev. **127**, 1918 (1962).

[3] R. W. Minck, R. W. Terhune, and C. C. Wang, Nonlinear optics, Appl. Opt. **5**, 1595 (1966).

[4] Y. R. Shen, Recent advances in nonlinear optics, Rev. Mod. Phys. **48**, 1 (1976).

[5] N. Bloembergen, Nonlinear optics and spectroscopy, Rev. Mod. Phys. **54**, 685 (1982).

[6] J. A. Hermann and D. F. Walls, Theory of two-photon optical tristability, Phys. Rev. A **26**, 2085 (1982).

[7] L. A. Lugiato, II Theory of optical bistability, Prog. Opt. **21**, 69 (1984).

[8] G. Lenz, P. Meystre, and E. M. Wright, Nonlinear Atom Optics, Phys. Rev. Lett. **71**, 3271 (1993).

[9] J. Gripp, S. L. Mielke, L. A. Orozco, and H. J. Carmichael, Anharmonicity of the vacuum Rabi peaks in a many-atom system, Phys. Rev. A **54**, R3746(R) (1996).

[10] Y. P. Svirko and N. I. Zheludev, *Polarization of Light in Nonlinear Optics* (Wiley, Chichester, 1998).

[11] G. Khitrova, H. M. Gibbs, F. Jahnke, M. Kira, and S. W. Koch, Nonlinear optics of normal-mode-coupling semiconductor microcavities, Rev. Mod. Phys. **71**, 1591 (1999).

[12] K. Koshino and H. Ishihara, Evaluation of Two-Photon Nonlinearity by a Semiclassical Method, Phys. Rev. Lett. **93**, 173601 (2004).

[13] S. Gupta, K. L. Moore, K. W. Murch, and D. M. Stamper-Kurn, Cavity Nonlinear Optics at Low Photon Numbers from Collective Atomic Motion, Phys. Rev. Lett. **99**, 213601 (2007).

[14] A. Dombi, A. Vukics, and P. Domokos, Optical bistability in strong-coupling cavity QED with a few atoms, J. Phys. B **46**, 224010 (2013).

[15] V. V. Konotop, J. Yang, and D. A. Zezyulin, Nonlinear waves in PT-symmetric systems, Rev. Mod. Phys. **88**, 035002 (2016).

[16] H. Zoubi and K. Hammerer, Quantum Nonlinear Optics in Optomechanical Nanoscale Waveguides, Phys. Rev. Lett. **119**, 123602 (2017).

[17] A. Angerer, S. Putz, D. O. Krimer, T. Astner, M. Zens, R. Glattauer, K. Streltsov, W. J. Munro, K. Nemoto, S. Rotter, J. Schmiedmayer, and J. Majer, Ultralong relaxation times in bistable hybrid quantum systems, Sci. Adv. **3**, e1701626 (2017).

[18] G. Yumoto, R. Matsunaga, H. Hibino, and R. Shimano, Ultrafast Terahertz Nonlinear Optics of Landau Level Transitions in a Monolayer Graphene, Phys. Rev. Lett. **120**, 107401 (2018).

[19] D. O. Krimer, M. Zens, and S. Rotter, Critical phenomena and nonlinear dynamics in a spin ensemble strongly coupled to a cavity. I. Semiclassical approach, Phys. Rev. A **100**, 013855 (2019).

[20] P. D. Drummond and D. F. Walls, Quantum theory of optical bistability. I. Nonlinear polarisability model, J. Phys. A **13**, 725 (1980).

[21] H. Risken, C. Savage, F. Haake, and D. F. Walls, Quantum tunneling in dispersive optical bistability, Phys. Rev. A **35**, 1729 (1987).

[22] J. P. Torres, J. Boyce, and R. Y. Chiao, Bilateral Symmetry Breaking in a Nonlinear Fabry-Pérot Cavity Exhibiting Optical Tristability, Phys. Rev. Lett. **83**, 4293 (1999).

[23] H. Rehbein, J. Harms, R. Schnabel, and K. Danzmann, Optical Transfer Functions of Kerr Nonlinear Cavities and Interferometers, Phys. Rev. Lett. **95**, 193001 (2005).

[24] F. Y. Wang, G. X. Li, H. L. Tam, K. W. Cheah, and S. N. Zhu, Optical bistability and multistability in one-dimensional periodic metal-dielectric photonic crystal, Appl. Phys. Lett. **92**, 211109 (2008).

[25] A. Khalaidovski, A. Thüring, H. Rehbein, N. Lastzka, B. Willke, K. Danzmann, and R. Schnabel, Strong reduction of laser power noise by means of a Kerr nonlinear cavity, Phys. Rev. A **80**, 053801 (2009).

[26] A. Thüring and R. Schnabel, Critical Kerr nonlinear optical cavity in the presence of internal loss and driving noise, Phys. Rev. A **84**, 033839 (2011).

[27] S. Ferretti and D. Gerace, Single-photon nonlinear optics with Kerr-type nanostructured materials, Phys. Rev. B **85**, 033303 (2012).

[28] S. Shahidani, M. H. Naderi, and M. Soltanolkotabi, Control and manipulation of electromagnetically induced transparency in a nonlinear optomechanical system with two movable mirrors, Phys. Rev. A **88**, 053813 (2013).

[29] S. Aldana, C. Bruder, and A. Nunnenkamp, Equivalence between an optomechanical system and a Kerr medium, Phys. Rev. A **88**, 043826 (2013).

[30] H. Z. Shen, Y. H. Zhou, and X. X. Yi, Tunable photon blockade in coupled semiconductor cavities, Phys. Rev. A **91**, 063808 (2015).

[31] J. Li, R. Yu, and Y. Wu, Proposal for enhanced photon blockade in parity-time-symmetric coupled microcavities, Phys. Rev. A **92**, 053837 (2015).

[32] W. Yu, P. Ma, H. Sun, L. Gao, and R. E. Noskov, Optical tristability and ultrafast Fano switching in nonlinear magnetoplasmonic nanoparticles, Phys. Rev. B **97**, 075436 (2018).

[33] M. D. Lukin and A. Imamoğlu, Nonlinear Optics and Quantum Entanglement of Ultraslow Single Photons, Phys. Rev. Lett. **84**, 1419 (2000).

[34] J. D. Franson, Photon exchange interactions and quantum information processing, Phys. Rev. A **70**, 054301 (2004).

[35] D. Vitali, S. Gigan, A. Ferreira, H. R. Böhm, P. Tombesi, A. Guerreiro, V. Vedral, A. Zeilinger, and M. Aspelmeyer, Optomechanical Entanglement between a Movable Mirror and a Cavity Field, Phys. Rev. Lett. **98**, 030405 (2007).

[36] J. L. O'Brien, Optical quantum computing, Science **318**, 1567 (2007).

[37] P. Adhikari, M. Hafezi, and J. M. Taylor, Nonlinear Optics Quantum Computing with Circuit QED, Phys. Rev. Lett. **110**, 060503 (2013).

[38] B. Bobbs, R. Shih, and H. R. Fetterman, Nonlinear microwave susceptibility measurement of an artificial Kerr medium, Appl. Phys. Lett. **52**, 4 (1988).

[39] M. D. Spirito, R. Pizzoferrato, U. Zammit, M. Marinelli, F. Scudieri, S. Martellucci, and M. Romagnoli, Third-order nonlinearity enhancement in an artificial Kerr medium through bulk intrinsic birefringence, Opt. Lett. **14**, 239 (1989).

[40] A. D. Boardman, P. J. Baldwin, J. E. McNiff, and Yu. G. Rapoport, Nonlinear response of microwave guides containing carbon-loaded composite materials, J. Phys. D **38**, 78 (2005).

[41] S. Rebić, J. Twamley, and G. J. Milburn, Giant Kerr Nonlinearities in Circuit Quantum Electrodynamics, Phys. Rev. Lett. **103**, 150503 (2009).

[42] M. Lapine, I. V. Shadrivov, and Y. S. Kivshar, Colloquium: Nonlinear metamaterials, Rev. Mod. Phys. **86**, 1093 (2014).
[43] Y. P. Wang, G. Q. Zhang, D. K. Zhang, X. Q. Luo, W. Xiong, S. P. Wang, T. F. Li, C.-M. Hu, and J. Q. You, Magnon Kerr effect in a strongly coupled cavity-magnon system, Phys. Rev. B **94**, 224410 (2016).
[44] Y. P. Wang, G. Q. Zhang, D. K. Zhang, T. F. Li, C.-M. Hu, and J. Q. You, Bistability of Cavity Magnon Polaritons, Phys. Rev. Lett. **120**, 057202 (2018).
[45] P. Hyde, B. M. Yao, Y. S. Gui, G. Q. Zhang, J. Q. You, and C.-M. Hu, Direct measurement of foldover in cavity magnon-polariton systems, Phys. Rev. B **98**, 174423 (2018).
[46] G. Q. Zhang, Y. P. Wang, and J. Q. You, Theory of the magnon Kerr effect in cavity magnonics, Sci. China: Phys., Mech. Astron. **62**, 987511 (2019).
[47] C. Kong, H. Xiong, and Y. Wu, Magnon-Induced Nonreciprocity Based on the Magnon Kerr Effect, Phys. Rev. Appl. **12**, 034001 (2019).
[48] Z. Zhang, M. O. Scully, and G. S. Agarwal, Quantum entanglement between two magnon modes via Kerr nonlinearity driven far from equilibrium, Phys. Rev. Res. **1**, 023021 (2019).
[49] Ö. O. Soykal and M. E. Flatté, Strong Field Interactions between a Nanomagnet and a Photonic Cavity, Phys. Rev. Lett. **104**, 077202 (2010).
[50] H. Huebl, C. W. Zollitsch, J. Lotze, F. Hocke, M. Greifenstein, A. Marx, R. Gross, and S. T. B. Goennenwein, High Cooperativity in Coupled Microwave Resonator Ferrimagnetic Insulator Hybrids, Phys. Rev. Lett. **111**, 127003 (2013).
[51] Y. Tabuchi, S. Ishino, T. Ishikawa, R. Yamazaki, K. Usami, and Y. Nakamura, Hybridizing Ferromagnetic Magnons and Microwave Photons in the Quantum Limit, Phys. Rev. Lett. **113**, 083603 (2014).
[52] M. Goryachev, W. G. Farr, D. L. Creedon, Y. Fan, M. Kostylev, and M. E. Tobar, High-Cooperativity Cavity QED with Magnons at Microwave Frequencies, Phys. Rev. Appl. **2**, 054002 (2014).
[53] B. Bhoi, T. Cliff, I. S. Maksymov, M. Kostylev, R. Aiyar, N. Venkataramani, S. Prasad, and R. L. Stamps, Study of photon–magnon coupling in a YIG-film split-ring resonant system, J. Appl. Phys. **116**, 243906 (2014).
[54] X. Zhang, C.-L. Zou, L. Jiang, and H. X. Tang, Strongly Coupled Magnons and Cavity Microwave Photons, Phys. Rev. Lett. **113**, 156401 (2014).
[55] L. Bai, M. Harder, Y. P. Chen, X. Fan, J. Q. Xiao, and C.-M. Hu, Spin Pumping in Electrodynamically Coupled Magnon-Photon Systems, Phys. Rev. Lett. **114**, 227201 (2015).
[56] D. Zhang, X.-M. Wang, T.-F. Li, X.-Q. Luo, W. Wu, F. Nori, and J. You, Cavity quantum electrodynamics with ferromagnetic magnons in a small yttrium-iron-garnet sphere, npj Quantum Inf. **1**, 15014 (2015).
[57] Y. Cao, P. Yan, H. Huebl, S. T. B. Goennenwein, and G. E. W. Bauer, Exchange magnon-polaritons in microwave cavities, Phys. Rev. B **91**, 094423 (2015).
[58] J. A. Haigh, N. J. Lambert, A. C. Doherty, and A. J. Ferguson, Dispersive readout of ferromagnetic resonance for strongly coupled magnons and microwave photons, Phys. Rev. B **91**, 104410 (2015).
[59] B. Z. Rameshti, Y. Cao, and G. E. W. Bauer, Magnetic spheres in microwave cavities, Phys. Rev. B **91**, 214430 (2015).
[60] L. V. Abdurakhimov, Yu. M. Bunkov, and D. Konstantinov, Normal-Mode Splitting in the Coupled System of Hybridized Nuclear Magnons and Microwave Photons, Phys. Rev. Lett. **114**, 226402 (2015).
[61] B. M. Yao, Y. S. Gui, Y. Xiao, H. Guo, X. S. Chen, W. Lu, C. L. Chien, and C.-M. Hu, Theory and experiment on cavity magnon-polariton in the one-dimensional configuration, Phys. Rev. B **92**, 184407 (2015).
[62] H. Maier-Flaig, M. Harder, R. Gross, H. Huebl, and S. T. B. Goennenwein, Spin pumping in strongly coupled magnon-photon systems, Phys. Rev. B **94**, 054433 (2016).
[63] J. Bourhill, N. Kostylev, M. Goryachev, D. L. Creedon, and M. E. Tobar, Ultrahigh cooperativity interactions between magnons and resonant photons in a YIG sphere, Phys. Rev. B **93**, 144420 (2016).
[64] H. H. Jiang, Y. Xiao, C.-M. Hu, H. Guo, and K. Xia, Effect of magnetization boundary condition on cavity magnon polariton of YIG thin film, Nanotechnology **29**, 254002 (2018).
[65] Y. Xiao, X. H. Yan, Y. Zhang, V. L. Grigoryan, C. M. Hu, H. Guo, and K. Xia, Magnon dark mode of an antiferromagnetic insulator in a microwave cavity, Phys. Rev. B **99**, 094407 (2019).
[66] G. Q. Zhang and J. Q. You, Higher-order exceptional point in a cavity magnonics system, Phys. Rev. B **99**, 054404 (2019).
[67] W. C. Yu, J. J. Wang, H. Y. Yuan, and J. Xiao, Prediction of Attractive Level Crossing via a Dissipative Mode, Phys. Rev. Lett. **123**, 227201 (2019).
[68] M. Goryachev, S. Watt, J. Bourhill, M. Kostylev, and M. E. Tobar, Cavity magnon polaritons with lithium ferrite and three-dimensional microwave resonators at millikelvin temperatures, Phys. Rev. B **97**, 155129 (2018).
[69] M. X. Bi, X. H. Yan, Y. Xiao, and C. J. Dai, Magnon dark mode in a strong driving microwave cavity, J. Appl. Phys. **126**, 173902 (2019).
[70] D. F. Walls and G. J. Milburn, *Quantum Optics* (Springer, Berlin, 1994).
[71] J. R. Macdonald, Ferromagnetic resonance and the internal field in ferromagnetic materials, Proc. Phys. Soc. London, Ser. A **64**, 968 (1951).
[72] D. D. Stancil and A. Prabhakar, *Spin Waves: Theory and Applications* (Springer, Berlin, 2009).